Graft of cardiac progenitors in a pig model of right ventricular failure triggers myocardial epimorphosis, regeneration and protection of function

Lambert V[1], Deleris A[2], Tibourtine[2], F, Fouilloux[3,2] V, Martin, A[4], Bridge, P[5], Aries E[3], Benoist, D[5], Pucéat, M[2]

[1]Paediatric and Congenital Cardiology, Department of Cardiology, Institut Mutualiste Montsouris, Paris, France ; [2]INSERM U1251/MMG, Aix-Marseille University, Marseille ; [3]Department of Pediatric Cardiac Surgery, Aix-Marseille University, Marseille, France.[4] Department of Congenital Cardiac Surgery, Bordeaux University, Pessac- Bordeaux, France Laboratoire Imagerie Interventionnelle Experimentale CERIMED, Marseille,[5] Liryc – the Electrophysiology and Heart Modelling Institute, Pessac-Bordeaux, France

Correspondence: michel.puceat@inserm.fr

The failure of diseased adult heart to regenerate is a major burden to our societies. Besides patients with ischemia and left ventricular (LV) dysfunction, progress in pediatric surgery to repair cardiac malformations has led to a growing population of now adult congenital heart diseases (CHD) patients with right ventricular (RV) failure. In the absence of any efficient pharmacological therapy for these patients, cell therapy has turned out to be the only option to regenerate the RV myocardium.

In this study, we demonstrate that the adult pig with RV failure, a model of repaired tetralogy of Fallot, has the ability of regenerative epimorphosis.

Human embryonic stem cell-derived cardiac Nkx2.5+ progenitor cells were seeded in a collagen based patch to cover the whole pig failing RV. We report that these cells migrate within the myocardium while reversing the interstitial fibrosis. They then engraft and fully differentiate into fetal-like human myocytes within the myocardium. The graft triggers the reprogramming of surrounding pig myocytes into Oct4+ cells. The reprogrammed myocytes re-differentiate and proliferate around human myocytes. Altogether, our findings reveal that mammalian hearts have the ability to undergo epimorphosis, the major process of endogenous regeneration that leads to a recovery of their contractile function.

Congenital heart diseases (CHD) are the major developmental diseases[1]. Significant and continuous progress in pediatric surgery from the 1990's to repair cardiac malformations has greatly improved the survival of children who now constitutes a growing population of adult CHD patients. In this specific population, RV dysfunction typically develops as a consequence of chronic pressure and/or volume overload which is secondary to the originally lifesaving surgical repair procedures[2]. Then, these young adult patients with grown up congenital heart (GUCH) diseases are at high risk of heart failure, severe arrhythmias, valve disease, pulmonary hypertension, cancer and potentially early aging[3,4], which constitutes a medical burden[2,5]. Since more than 50% of GUCH patients have a risk of heart failure at 30 years old[6], RV failure makes the long-term follow-up of CHD a challenging medical issue.

The RV is thin, features a gene profile different from the LV and a maladaptive metabolic response to afterload[7], making it less equipped than LV to respond to overload. Furthermore, therapeutic options for this disease remain poorly investigated[5] and conventional therapeutic pharmacological approaches for these patients are often disappointing[8]. In the long run, if the repair of causal myocardial lesions does not allow for an improvement in function, or if RV is a single ventricular heart such as in the hypoplastic left heart syndrome, organ transplantation is the only remaining option for these young patients. The difficulty and time to obtain heart grafts because of shortage of donors as well as the risk of such a heavy surgery for these young patients often severely affected[9] urgently calls for the search for alternative therapeutic pathways. Despite challenges which still need to be met, regenerative medicine still appears to be a powerful approach to prevent and treat terminal heart failure and its consequences[10].

Clinical trials of cell therapy for congenital heart disease are still rare[11,12]. The cell and molecular mechanisms as well as long term effects of that approach remained however unclear.

The aims of our study performed on a large animal model of CHD was to evaluate the therapeutic potential of an epicardial delivery of human embryonic stem cells-derived cardiac progenitor cells (CPC) in a porcine model of chronic overloaded RV dysfunction[13] and to uncover the cellular and molecular mechanisms underlying the action of grafted cells.

To test the therapeutic effect of the graft of CPC, we performed heart surgery on 18 pigs in order to mimic the clinical situation of repaired TOF[13]. Four animals died during the study: three from the sham group (one severe cardiac failure, two ventricular fibrillations), one from the control group (infection) before the end of the follow-up, and they were excluded from the final analysis. All remaining animals (n=6-8/group) gained weight and did

not feature any clinical signs of heart failure. Age, weight, body length, and body surface area were similar in all groups at each stage (Fig. S1, Table 1). The time between the surgery and the delivery of epicardial patches was similar between CPC seeded patch and cell-free groups (206.0 ± 24.8 *vs* 211.5 ± 40.7 days respectively) as well as the whole duration of the experiment (296.3±17.4 *vs* 292.8± 23.2 days respectively). No mortality was observed after cell delivery, or during the follow-up, and no adverse effects occurred. Immunosuppression was well tolerated. In the post cell therapy period, all animals gained weight (Fig S1B, Table 1) and did not feature any clinical signs of either heart failure or immune rejection.

CPC were generated from the human embryonic stem cell line H9 genetically modified to express the ventricular myosin light chain 2 (MLC2v) fused to GFP[14] under the control of the cardiac α-actin promoter. Cells were sequentially challenged with a series of small molecules and growth factors (i.e, Wnt activator and BMP2 and then Wnt inhibitor and SHH) to direct them toward the fate of cardiac progenitors expressing NKX2.5 (Fig 1A)[15]. Cells were then sorted with an anti-CD15 antibody directed against an antigen (SSEA-1) expressed at the surface of differentiated cells[16] (Fig. 1A).

When grafted within the collagen based patch covering the whole right ventricle of pigs, the cells expressing phospho-histone 3 (PH3) still proliferated and were in the process of differentiation toward actinin+ cardiomyocytes within the patch two months after the graft (Fig 1B). However, most of cells migrated into the myocardium while differentiating into cardiomyocytes expressing the human nuclear antigen KU80 and fused MLC2vGFP protein within the sarcomeres. Migration was likely accompanied with a degradation of fibrosis allowed by expression of metalloproteases (i.e. MMP1 and TIMP1) by the CPC (Fig. S2). Interestingly, pig myocytes surrounding the human cardiomyocytes expressed NKX2.5, a transcription factor not any longer expressed in adult myocytes (Fig 1C,D).

We next investigated the effect of the graft of human CPC on the extent of fibrosis of the right ventricle. Pig hearts grafted with a cell-free patch still featured extended interstitial fibrosis as revealed by Sirius red staining (Fig 1D). In contrast, pig hearts grafted with CPC-cellularized patches featured a restricted or no longer fibrosis (Fig 1D).

To further evaluate the reversal in the extent of fibrosis in human CPC-grafted right ventricle, we carried out RT-QPCR of genes expressed in fibroblasts or myofibroblasts. Expression of both *Col1a2* and *Col3a1* genes was significantly decreased in CPC-grafted hearts when compared to cell–free patch grafted right ventricle. Periostin (*Postn*) expressed in fibroblasts and smooth muscle actin (*acta2*) expressed in myofibroblasts as well as the pro-fibrotic growth factor *TGFβ* were all downregulated in CPC-grafted right ventricles (Fig 1E).

Five months after surgery, echocardiography revealed in the two groups a similar combined RV overload. A significant thickening of the RV free wall secondary to a moderate but significant pulmonary stenosis reflected a barometric overload, associated with a pronounced RV dilatation (volumetric overload) assessed by increased RV/LV ratio, indexed diastolic diameter and both end-diastolic and end-systolic areas, following a severe pulmonary regurgitation (table 1, Fig.2). Echocardiographic standard parameters such as indexed TAPSE and peak systolic velocity of S'wave, as well as myocardial strain measures, significantly decreased to the same extent in the two groups; these results showed an alteration of both global RV function and myocardial contractility. Two months after patch delivery, indexed RV diameter significantly decreased in the CPC group whereas it increased in cell-free group. The free wall thickness significantly increased in the CPC group compared to cell-free group. These results suggest that the RV adaptation to the overload was maintained. The global RV function was maintained in the CPC group while it decreased in the cell-free group. Furthermore, the myocardial contractility specifically assessed by free wall strain significantly improved in the CPC group in contrast to cell-free group in which it kept decreasing. Then, functional characteristics and contractility parameters differently evolved after either with or without cardiac progenitors (Fig 2).

In order to understand the improved RV function in CPC-grafted pigs, we screened for proliferative cells within the right ventricle grafted with cell-free or CPC–containing patches. While we did not detect any cycling cells in hearts grafted with cell free patches, PH3+ and Nkx2.5+ cells were found in interstitial tissues of CPC grafted ventricles. The cells further featured some immature actinin containing sarcomeres (Fig 3A). We next used another marker of cell proliferation, i.e. Ki67 as an index of DNA-duplicating cells. The anti Ki67 antibody revealed the presence of clusters of pig cells expressing at the membrane Troponin T in nascent sarcomeres within the fibrotic area. These cells were not GFP+ and were not stained by the human specific mitochondria antibody confirming that they were pig cells (Fig 4B).

This intriguing observation led us to further investigate the phenotype of pig myocytes surrounding the human MLC2vGFP+ cardiomyocytes within the heart. Measurement of the size of sarcomeres revealed significantly shorter fetal like sarcomeres in pig myocytes neighbor of human cardiomyocytes than myocytes away from this area. Human myocytes also featured short fetal-like sarcomeres as expected from their still immature phenotype (Fig 3C,D).

As adult cardiomyocytes do not reenter the cell cycle, we wondered how pig fetal like myocytes could have been generated around grafted human cardiomyocytes. We thus raised the hypothesis that pig myocytes could have de-differentiated and re-differentiated following reactivation of an embryonic genetic program. We thus looked for one of the major markers of pluripotent naïve stem cells, namely Oct4. Figure 3E reveals that some pig myocytes of CPC-grafted RV but not of cell-free patch grafted RV expressed OCT4 (Fig 5A). OCT4 was localized into the nucleus, thus likely to be transcriptionally active (Fig 3E, inset). Some cells also expressed NFκB or both nuclear OCT4 and peri-nuclear NFκB (Fig 3F).

We thus reasoned that graft of CPC and their migration within the myocardium could trigger a local and restricted inflammation. Cytokines released within the environment could in principle activate NFκB pathway in either or both cardiac fibroblasts and cardiomyocytes. To test such a hypothesis, cardiac human fibroblasts were transfected with *p65/NFκB* cDNA. Ten days later NFκB+ cells expressed OCT4 (Fig S3A). Second neonatal post-mitotic mouse day 7 cardiomyocytes in primary culture were chosen for their capability to be transfected. *p65/NFκB* cDNA was transfected in the myocytes. One week later, colonies of OCT4+ cells were observed in the culture (Fig S3B). These dedifferentiated cells re-differentiated into cardiomyocytes as indicated by re-expression of actinin set in still immature sarcomeres (Fig S3B). Interleukin 6 activation of myocytes also led to a dose dependent reprogramming in OCT4+ cells (Fig S4).

We next hypothesized that a local inflammation should be mediated by resident immune cells. Macrophages have been involved in tissue regeneration[17] in many non-mammalian organisms. They are part of cardiac resident immune cells including in heart[18]. We thus tested the presence of macrophages in pig hearts. While a few macrophages could be found in RV grafted with cell-free patches (Fig 4A), pig hearts grafted with CPC revealed the presence of many iba1+ macrophages and more specifically around the graft of human MLC2vGFP myocytes (Fig 4B,C). The immune cells were adherent to pig cardiomyocytes (Fig 4B) and 3D- reconstruction of a z-stack of images even shows that they are integrated within the cardiac fibers (inset Figure 4B) allowing for a close interaction and dialog with the myocytes.

Here, we demonstrate that the epicardial delivery of cardiac progenitors in pigs with right ventricular failure, triggers reprogramming of pig cardiomyocytes into Oct4+ cells that re-differentiate into ventricular myocytes and regenerate the myocardium. The cells allow fibrosis to be reversed and improve index of contractility of the ventricle following a true myocardial regeneration process.

The pigs used in this study were 6-7 months old at the time of cell grafting thus far from the regenerative post-birth windows[19,20]. Furthermore the *in-vivo* myocyte reprogramming was triggered by a cell-cell interactions and endogenous cytokines without delivery of any pluripotency genes previously reported to trigger the same process[21].

The role of inflammation and specifically macrophages in tissue regeneration is not entirely new[22,23] but the cell and molecular mechanisms have not been well documented specifically for myocardial regeneration. It has furthermore never been directly associated with a cell therapy approach or involved in a process of *in vivo* cell reprogramming.

We now show that the primary event and the trigger of myocardial regeneration is the migration of cardiac progenitor cells from the epicardial patch towards the myocardium. The cells that underwent epithelial-to-mesenchymal transition earlier in the process of differentiation, an event required for their migration recapitulating the embryonic scenario indeed have the proteolytic equipment (Fig S2) to degrade the proteins of the extracellular matrix. They thus make their own path toward the myocardium through the interstitial fibrosis while differentiating (Fig 1). The degraded proteins thus add to the damaged associated molecular patterns (DAMP) likely constituted of components of dead myocytes or released by them such as ATP. This triggers an inflammatory process as revealed by the presence of NFκB expressing cells (Fig 3) still present two months after cell delivery. Interestingly many cells including fibroblasts and cardiomyocytes feature DAMP-sensing receptors[24] making the scenario likely.

The activated NFκB pathway in cardiomyocytes triggers a re-expression of the pluripotency factor Oct4 as revealed by immunofluorescence of CPC-grafted right ventricular sections (Fig 3). That NFκB is sufficient to induce Oct4 and to reprogram both cardiac fibroblasts and myocytes was revealed by our in vitro cell transfection assays (Fig S3) and as we previously reported for valvular cells[25]. Interestingly, the OCT4+ cells are capable to re-differentiate into myocytes both *in-vivo* and *in-vitro* (Fig 3 and S3) likely because of their environment and their epigenetic memory that they retained.

The immune cell involved is likely to be a macrophage often reported as a pro-regenerative and tissue repair cell. We found that Iba1+ macrophages did sit on cardiomyocytes and are clustered in RV grafted with CPC around the graft, which suggests their activated state (Fig 4). They thus have a privileged location to interact and dialog with cardiomyocytes and in turn to secrete their cytokines in their vicinity. Which macrophage plays that role is still not yet known under our experimental situation. We can however surmise that it could be a CCR2$^-$ macrophage of embryonic origin known to play a role in pediatric heart regeneration[18,23,26]. Lavine et al[23] have reported that embryonic macrophages are replaced by pro-inflammatory monocytes in adult post myocardial infarcted (MI) mouse hearts. However our pig model of RV failure with interstitial fibrosis is different from a mouse MI model with a scar. Furthermore Pig macrophages are transcriptionally more close to human, than mouse immune cells[27]. Local activation of CCR2$^-$ macrophages within the interstitial fibrosis is still very likely and experiments of spatial transcriptomics and proteomics should clear up this issue.

How NFκB and cardiac inflammasome do reprogram pig myocytes without triggering an adverse inflammatory process remains to be elucidated. The location and the intimate dialog of resident macrophages with myocytes could in part answer the question. Furthermore, NFκB acts as a pioneer factor and likely requires another transcription factor to bind super-enhancer on *Oct4* gene regulatory regions[28]. It acts as a dosage dependent manner and its target-genes depend upon the frequency and amplitude of its intracellular oscillations[28,29]. Thus a time-dependent fine tuning regulation of activation of NFκB likely allows for cell reprogramming *versus* inflammation and fibrosis.

Microglia (i.e macrophages) that are also from embryonic origin[30] have been recently reported to promote adult brain repair, an event mediated by an IL6 pro-regenerative pathway[31] even if the full mechanism of the regeneration was not investigated.

Dedifferentiation or even reverse differentiation into stem cells as reported herein could be an efficient means to organ regeneration as previously reported and debated[32,33]. This is as more important and even facilitated for organs such as the hearts that lack stem cells, which could compete with such a process[32]. Thus such a macrophage-induced cell reprogramming or reverse differentiation could be a general cell mechanism to be explored in regenerative medicine.

ACKNOWLEGMENTS

We are very grateful to de Federation Francaise de Cardiologie (To VL, MP) and The Leducq Foundation which funded this work (SHAPEHEART network of excellence) and for generously awarding us for cell imaging facility (MP “Equipement de Recherche et Plateformes Technologiques” (ERPT)). We thank Drs Serge Van de Pavert and Serge Bajenoff (Centre Immulogie de Marseille-Luminy) for fruitful and helpful discussions.

REFERENCES

1 Hoffman, J. I. & Kaplan, S. The incidence of congenital heart disease. *J Am Coll Cardiol* **39**, 1890-1900, doi:10.1016/s0735-1097(02)01886-7 (2002).

2 Lopez, L. *et al.* Unnatural history of the right ventricle in patients with congenitally malformed hearts. *Cardiol Young* **20 Suppl 3**, 107-112, doi:10.1017/S1047951110001150 (2010).

3 Diller, G. P. *et al.* Lifespan Perspective on Congenital Heart Disease Research: JACC State-of-the-Art Review. *J Am Coll Cardiol* **77**, 2219-2235, doi:10.1016/j.jacc.2021.03.012 (2021).

4 Moons, P. M., A. Born to Age: when adult congenital heart disease converges with Geroscience. *JACC: advances* **1**, &-12 (2022).

5 Wang, F. *et al.* Heart failure risk predictions in adult patients with congenital heart disease: a systematic review. *Heart* **105**, 1661-1669, doi:10.1136/heartjnl-2019-314977 (2019).

6 Norozi, K. *et al.* Incidence and risk distribution of heart failure in adolescents and adults with congenital heart disease after cardiac surgery. *Am J Cardiol* **97**, 1238-1243, doi:10.1016/j.amjcard.2005.10.065 (2006).

7 Garcia, A. M., Beatty, J. T. & Nakano, S. J. Heart failure in single right ventricle congenital heart disease: physiological and molecular considerations. *Am J Physiol Heart Circ Physiol* **318**, H947-H965, doi:10.1152/ajpheart.00518.2019 (2020).

8 Reddy, S. & Bernstein, D. Molecular Mechanisms of Right Ventricular Failure. *Circulation* **132**, 1734-1742, doi:10.1161/CIRCULATIONAHA.114.012975 (2015).

9 Cohen, S. & Marelli, A. Evolving heart transplantation across the lifespan: A growing population of adults with congenital heart disease. *Arch Cardiovasc Dis* **109**, 511-513, doi:10.1016/j.acvd.2016.05.001 (2016).

10 Murry, C. E. & MacLellan, W. R. Stem cells and the heart-the road ahead. *Science* **367**, 854-855, doi:10.1126/science.aaz3650 (2020).

11 Abdullah, M. *et al.* Stem Cell Therapy in Single-Ventricle Physiology: Recent Progress and Future Directions. *Semin Thorac Cardiovasc Surg Pediatr Card Surg Annu* **24**, 67-76, doi:10.1053/j.pcsu.2021.03.003 (2021).

12 Bittle, G. J. *et al.* Stem Cell Therapy for Hypoplastic Left Heart Syndrome: Mechanism, Clinical Application, and Future Directions. *Circ Res* **123**, 288-300, doi:10.1161/CIRCRESAHA.117.311206 (2018).

13 Lambert, V. *et al.* Right ventricular failure secondary to chronic overload in congenital heart disease: an experimental model for therapeutic innovation. *The Journal of thoracic and cardiovascular surgery* **139**, 1197-1204, 1204 e1191, doi:10.1016/j.jtcvs.2009.11.028 (2010).

14 Grey, C., Mery, A. & Puceat, M. Fine-tuning in Ca2+ homeostasis underlies progression of cardiomyopathy in myocytes derived from genetically modified embryonic stem cells. *Human molecular genetics* **14**, 1367-1377, doi:10.1093/hmg/ddi146 (2005).

15 Jebeniani, I., Ding, S. & Puceat, M. Improved Protocol for Cardiac Differentiation and Maturation of Pluripotent Stem Cells. *Methods Mol Biol* **1994**, 71-77, doi:10.1007/978-1-4939-9477-9_6 (2019).

16 Blin, G., Neri, T., Stefanovic, S. & Puceat, M. Human embryonic and induced pluripotent stem cells in basic and clinical research in cardiology. *Current stem cell research & therapy* **5**, 215-226, doi:10.2174/157488810791824584 (2010).

17 Wynn, T. A., Chawla, A. & Pollard, J. W. Macrophage biology in development, homeostasis and disease. *Nature* **496**, 445-455, doi:10.1038/nature12034 (2013).

18 Bajpai, G. *et al.* The human heart contains distinct macrophage subsets with divergent origins and functions. *Nat Med* **24**, 1234-1245, doi:10.1038/s41591-018-0059-x (2018).

19 Velayutham, N. *et al.* Cardiomyocyte cell cycling, maturation, and growth by multinucleation in postnatal swine. *J Mol Cell Cardiol* **146**, 95-108, doi:10.1016/j.yjmcc.2020.07.004 (2020).

20 Velayutham, N. & Yutzey, K. E. Porcine Models of Heart Regeneration. *J Cardiovasc Dev Dis* **9**, doi:ARTN 9310.3390/jcdd9040093 (2022).

21 Chen, Y. P. *et al.* Reversible reprogramming of cardiomyocytes to a fetal state drives heart regeneration in mice. *Science* **373**, 1537-+, doi:10.1126/science.abg5159 (2021).
22 Cooke, J. P. Inflammation and Its Role in Regeneration and Repair. *Circ Res* **124**, 1166-1168, doi:10.1161/CIRCRESAHA.118.314669 (2019).
23 Lavine, K. J. *et al.* Distinct macrophage lineages contribute to disparate patterns of cardiac recovery and remodeling in the neonatal and adult heart. *Proc Natl Acad Sci U S A* **111**, 16029-16034, doi:10.1073/pnas.1406508111 (2014).
24 Gong, T., Liu, L., Jiang, W. & Zhou, R. DAMP-sensing receptors in sterile inflammation and inflammatory diseases. *Nat Rev Immunol* **20**, 95-112, doi:10.1038/s41577-019-0215-7 (2020).
25 Farrar, E. J. *et al.* OCT4-mediated inflammation induces cell reprogramming at the origin of cardiac valve development and calcification. *Sci Adv* **7**, eabf7910, doi:10.1126/sciadv.abf7910 (2021).
26 Epelman, S. *et al.* Embryonic and Adult-Derived Resident Cardiac Macrophages Are Maintained through Distinct Mechanisms at Steady State and during Inflammation. *Immunity* **40**, 91-104, doi:10.1016/j.immuni.2013.11.019 (2014).
27 Kapetanovic, R. *et al.* The impact of breed and tissue compartment on the response of pig macrophages to lipopolysaccharide. *BMC Genomics* **14**, 581, doi:10.1186/1471-2164-14-581 (2013).
28 Michida, H. *et al.* The Number of Transcription Factors at an Enhancer Determines Switch-like Gene Expression. *Cell Rep* **31**, 107724, doi:10.1016/j.celrep.2020.107724 (2020).
29 Cheng, Q. J. *et al.* NF-kappaB dynamics determine the stimulus specificity of epigenomic reprogramming in macrophages. *Science* **372**, 1349-1353, doi:10.1126/science.abc0269 (2021).
30 Ginhoux, F. *et al.* Fate mapping analysis reveals that adult microglia derive from primitive macrophages. *Science* **330**, 841-845, doi:10.1126/science.1194637 (2010).
31 Willis, E. F. *et al.* Repopulating Microglia Promote Brain Repair in an IL-6-Dependent Manner. *Cell* **180**, 833-+, doi:10.1016/j.cell.2020.02.013 (2020).
32 Tata, P. R. *et al.* Dedifferentiation of committed epithelial cells into stem cells in vivo. *Nature* **503**, 218-223, doi:10.1038/nature12777 (2013).
33 Shivdasani, R. A., Clevers, H. & de Sauvage, F. J. Tissue regeneration: Reserve or reverse? *Science* **371**, 784-786, doi:10.1126/science.abb6848 (2021).

TABLE 1: Population characteristics and echocardiographic parameters of RV morphology and systolic function in CPC and no-cell groups at each step of experimentation.

	Baseline		Follow-up			
			Patch application		*End point*	
	No cell n=6	**CPC n=8**	**No cell n=6**	**CPC n=8**	**No cell n=6**	**CPC n=8**
Population characteristics						
Age (days)	63.3 ± 19	62.9 ± 4.3	211.5 ± 40.7	206.0 ± 24.8	292.8± 23.2	296.3±17.4
Weight (kg)	20.0 ± 4.2	17.8 ± 4.2	77.7 ± 13.6	69.1±24.6	103.9±30.9	87.6 ± 26.7
Biological length (m)	0.77±0.08	0.74±0.07	1.23 ± 0.09	1.16 ± 0.13	1.36 ± 0.10	1.26 ± 0.12
BSA (m^2)	0.60±0.12	0.54±0.11	1.51 ±0.23	1.35 ± 0.3	1.86 ±0.28	1.60 ± 0.30
RV dimensions						
ED diameter/BL (mm/m)	18.3±3.7	19.0±4.0	24.6±3.5	25.6±5.9	28.2±7.5	22.3±3.9
RV/LV diameter ratio	0.42±0.11	0.40±0.10	0.71±0.10*	0.80±0.28*	0.88±0.27*	0.72±0.16*
ED area/BSA (cm/m^2)	8.3±1.7	8.9±1.1	9.1±2.7	11.1±5.7	10.2±3.9	8.4±2.9
ES area/BSA (cm/m^2)	4.3±1.3	4.8±0.7	5.2±2.4	6.4±3.7	6.0±3.3	4.7±1.7
T/M valve diameter ratio	0.86±0.12	0.85±0.08	1.05±0.08*	1.05±0.33	1.03±0.29	1.08±0.24*
RV/PA mean gradient (mmHg)	2.9±2.5	2.0±0.6	26.7±13.2*	17.9±8.7*	32.5±22.9*	17.5±9.0*
Free wall thickness (mm)	3.5±0.7	3.5±0.6	7.9±0.9*	7.3±1.6*	8.3±1.3*	10.6±2.8*†
RV systolic function						
FAC (%)	50.5±10.8	45.8±4.2	45.4±12.5*	43.3±5.0	41.6±12.6*	45.5±4.5
S' wave (cm/s)	8.7±2.3	8.9±2.8	9.4±1.9	10.2±3.6	9.6±4.6	10.2±2.4
TAPSE/BL (mm/m)	17.3±3.1	19.2±4.9	15.1±3.8	15.8±3.8	12.3±3.9	14.3±2.3
RV contractility						
Free wall strain (%)	24.5±3	24.8±3	19.7±3.*	18.1±6.0*	15.4±7.5*	21.3±6.9†
Global strain (%)	20.7±4.2	21.9±2.4	16.9±4.3	16.6±4.9	14.4±7.1	17.0±6.1

*Data are expressed as mean ± standard deviation; BSA, body surface area; BL: biological length (square root of BSA); ED, end-diastolic; ES, end-systolic; FAC, Fraction of Area Change; LV, Left ventricle; M, mitral; PA, Pulmonary artery; RV, right ventricle. T, tricuspid; TAPSE, Tricuspid Annular Plane Systolic Excursion; *p ≤ .05 versus corresponding group at baseline. †p ≤ .05, no-cell group versus CPC group at same step*

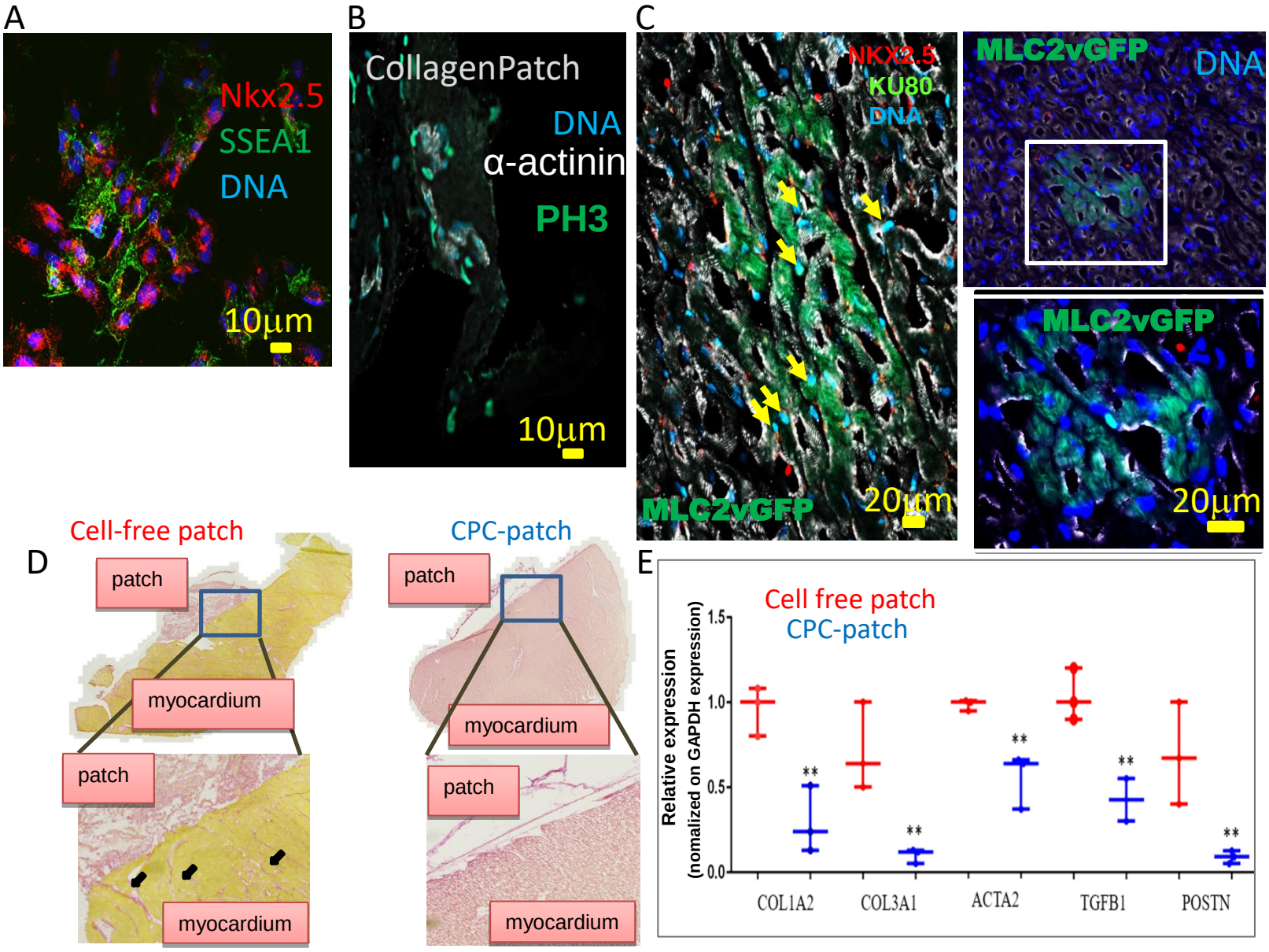

Fig. 1: Human ES cell-derived Nkx2.5+ cardiac progenitors migrate, differentiate within the RV myocardium and induce regression of fibrosis (**A**) human ES cell-derived Nkx2.5+ cardiac progenitors sorted using an anti-SSEA1 antibody (**B**) cells proliferate (PH3+) within the patch (**C**) migrate into and differentiate into clustered human KU80+ (light blue indicated by arrow) MLC2VGFP+ cardiomyocytes (**D**) Fibrosis is regressed in RV grafted with human cardiac progenitors. RV sections from pig grafted with an empty patch (Cell-free patch) or with a patch seeded with human cardiac progenitors (CPC-patch) stained with sirius red. Arrows indicate interstitial fibrosis . (**E**) Q-PCR of fibrosis related genes in either RV of pigs grafted with empty (cell-free) patchs or cellularized patchs (CPC patch) n=3 pigs. The images are representative of sections from 5 different pigs **t-Test $p<0.01$

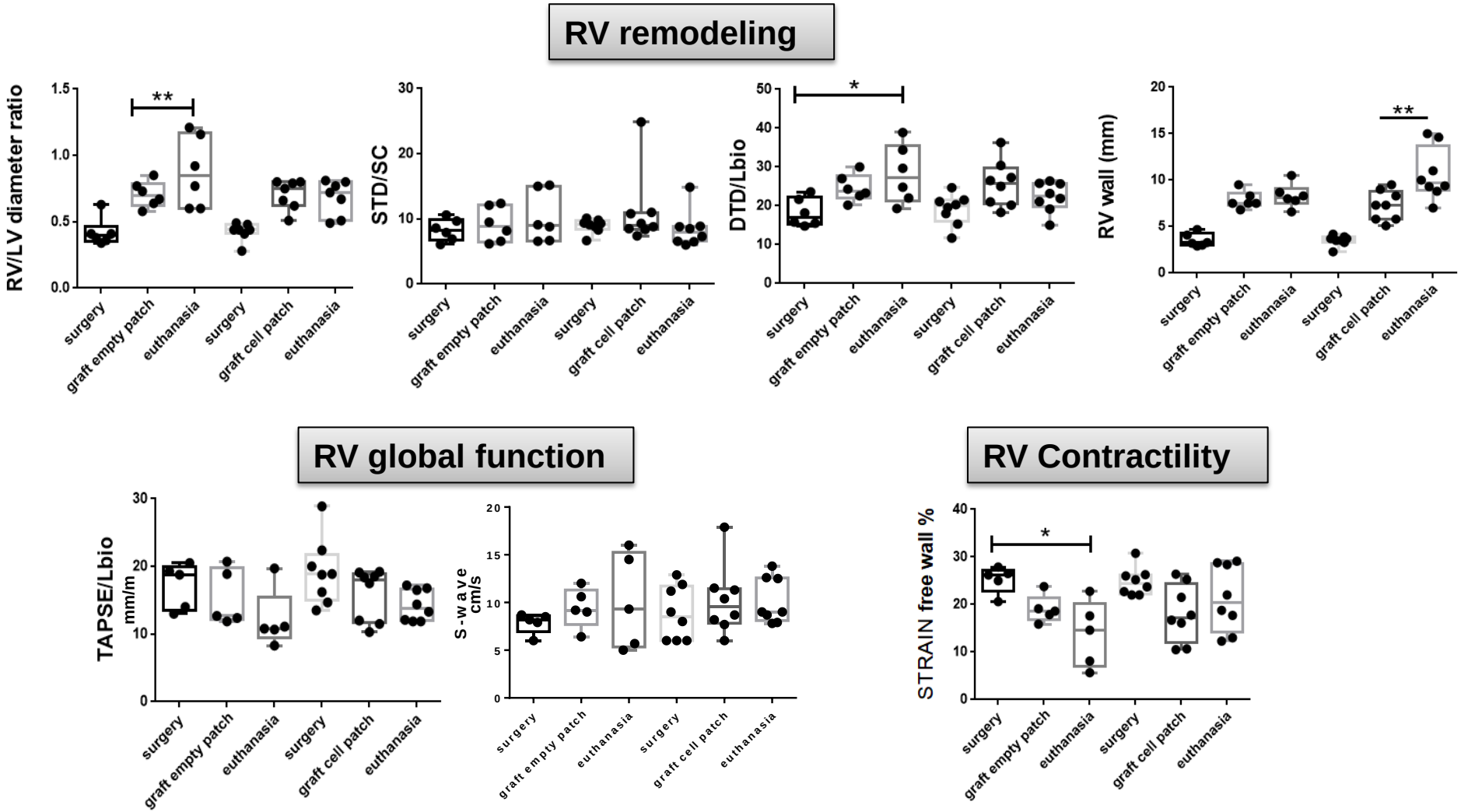

Figure 2: Functional parameters of pig grafted with cell-free patches (empty) or CPC –patch (cell) before the surgery (surgery), the day of the graft (graft) and at the end point of the experiment (euthanasia). The top graphs reflect the remodeling of the RV and the bottom ones, the contractility. T-test was used to compare two time points or Anova to compare 3 time points *p≤0.05 ** p ≤0.01

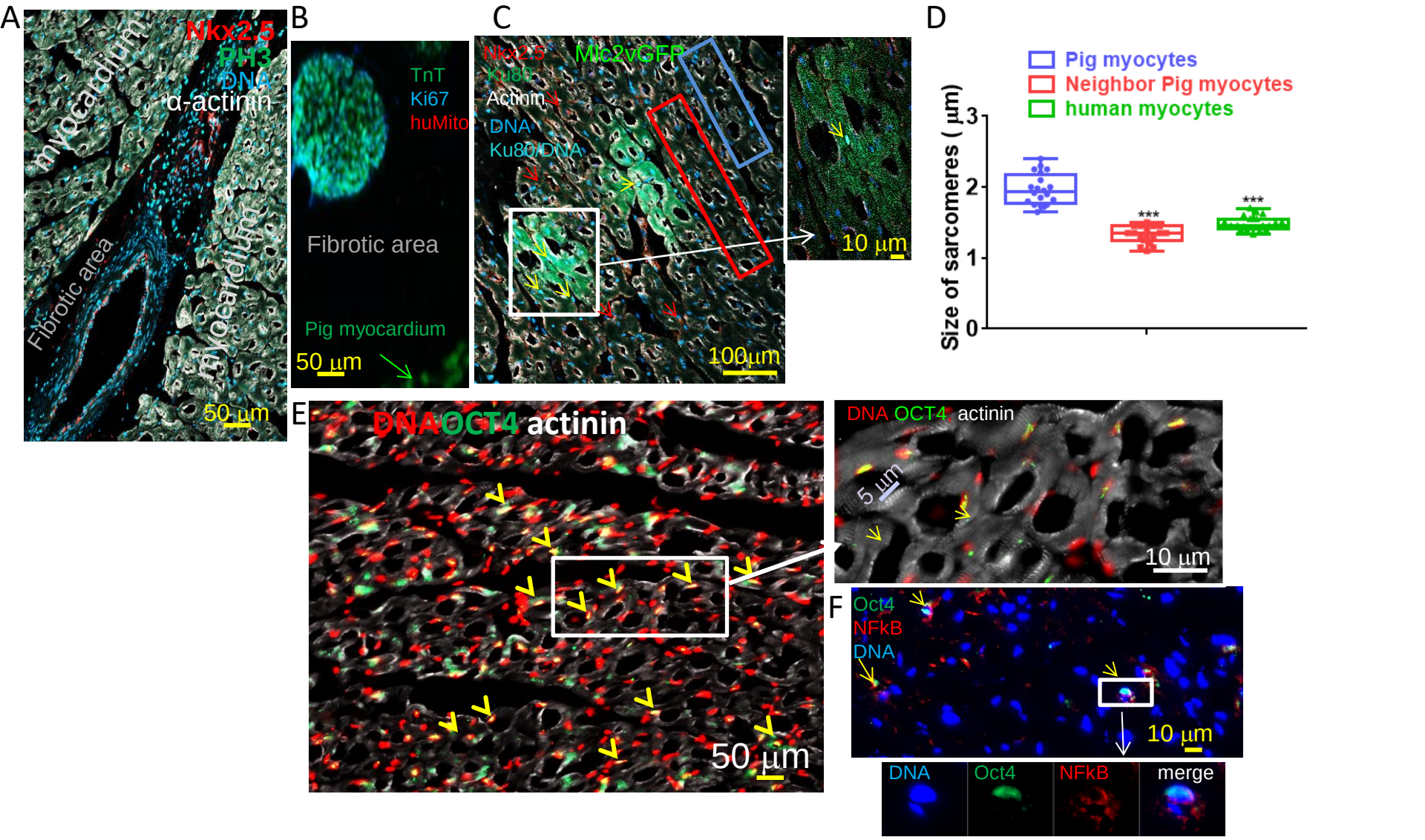

Fig 3: Pig myocytes are reprogrammed and reproliferate in human cardiac progenitor-grafted RV. Pig RV sections were stained with anti-Nkx2.5, -PH3, and -sarcomeric actinin antibodies (**A**) or with anti-troponin T (TnT), -Ki67 and -human Mitochondrial marker antibodies (**B**) or with anti-KU80, -Nkx2.5, and -sarcomeric actinin antibodies (**C**) the inset in C show high magnication. Human MLCGFP+ myocytes positive for KU80 (indicated by yellow arrows while nkx2.5+ nuclei are indicated by red arrows) (**D**): size of sarcomeres measured in pig myocytes far or close to human myocytes in 3 separate hearts. ***p<0.001. Cell-grafted RV sections were stained with anti-Oct4 and anti α-actinin antibodies. (**E**) Arrows point oct4+ cells. The inset shows a high magnification of cardiomyocytes. Sections were also stained with anti-Oct4 and anti-Nfkb antibodies (**F**). The inset shows a high magnification of Oct4+/Nfkb+ cells.The figure is representative of at least 4 different pigs grafted with cellularized CPC patch.

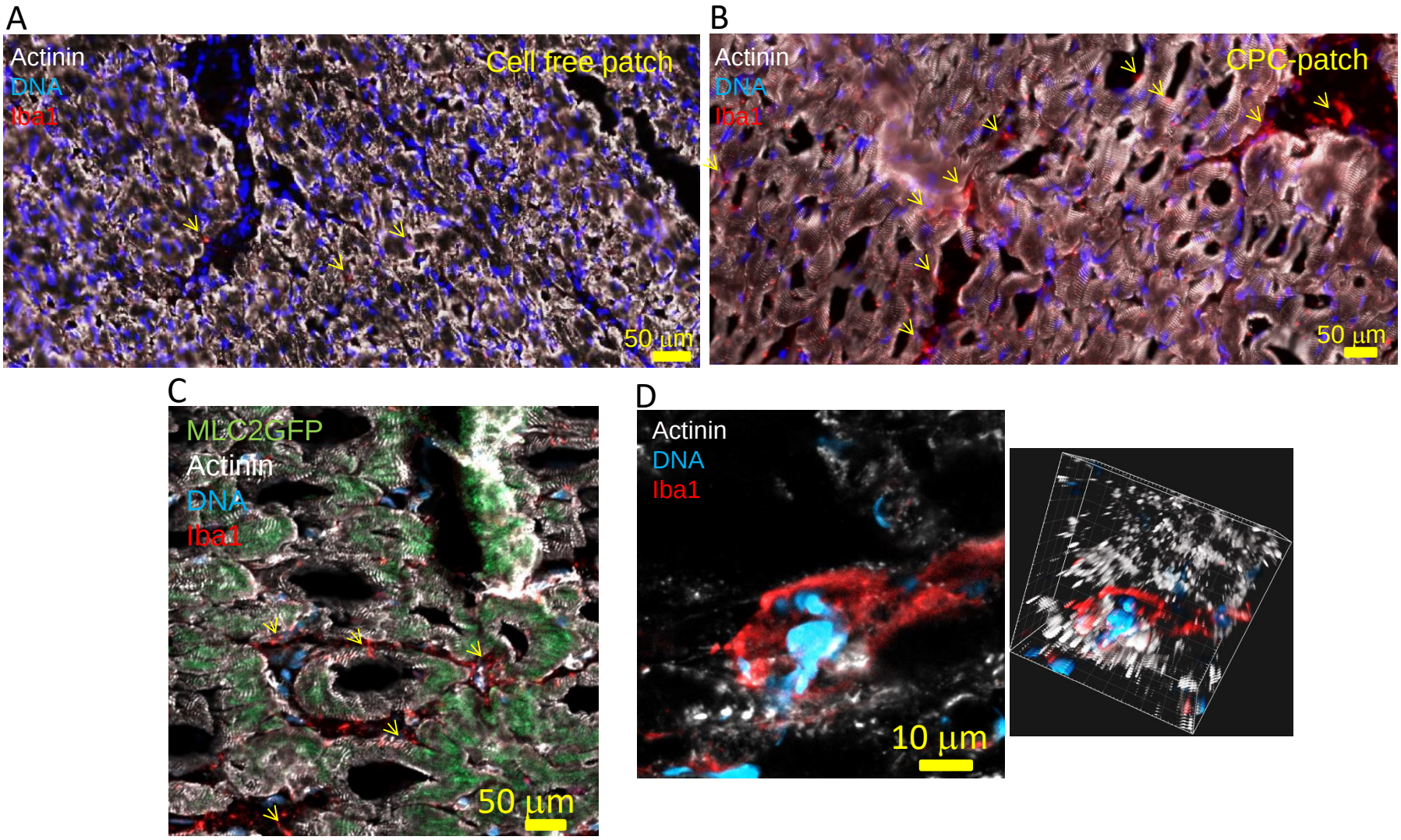

Fig. 4: Presence of macrophages on cardiomyocytes surrounding the graft. Macrophages (Iba1+) staining in RV section of pigs grafted with cell-free patch (**A**) or CPC- patch (**B**) Yellow arrows point to macrophages. (**C**) Immunofluorescence anti-Iba1 on RV section of pigs grafted with CPC-patches within the graft area (**D**) high magnification of Iba1+ macrophage on cardiac fibers. The right inset shows a 3D image reconstruction of the image revealing the position of the macrophage within the fiber.

MATERIALS AND METHODS

Genetic modification of HUES cells and cardiac differentiation

H9 HUES cell line was electroporated with a human α-actin pEGFP-C2 MLC2v DNA construct[1] and the clones selected using 100 μg/ml geneticin for 10 days.

Cells were differentiated as previously described[2]. Briefly, cells cultured on MEF were stimulated with 10 μM ChIR9901 for 14hrs (overnight) and then for 24 hrs with 5 μM ChIR9901 and 10 ng/ml BMP2, in RPMI medium supplemented with B27. The cells were further incubated with IWR1 10 μM and BMP2 for 24hrs and then with 2.5 μM IWP4 with 10 ng/ml BMP2 and finally for one more day with 2.5 μM IWP4 and 10 ng/ml SHH. Cells were then sorted using magnetic beads conjugated with an anti-CD15 antibody (clone MC-480) (Kit easy step, Stem cell Technology).

Cell Transfection

Human cardiac fibroblasts were from Promocell, (France). Neonatal mouse cardiomyocytes were isolated from 6 days old mice as previously reported[3] and isolated on a Percoll gradient. Both cell types were transfected in Optimem (ThermoFisher, France) using Trans IT (Mirus Bio) according to the manufacturer protocol.

Pig surgery and cell patch setting

All experiments were carried out according to the European Community guiding principles in

A surgical procedure mimicking repaired tetralogy of Fallot (rTOF) was performed on 18 Landrace male piglets of two months old to induce overloaded RV dysfunction. Briefly, an enlargement of the RV outflow tract by a polytetrafluoroethylene patch, excision of one pulmonary valve leaflet, and a pulmonary artery banding were performed through a left

thoracotomy approach[4]. After 5 months (median: 145 ± 22 days) of a combined pressure and volume overloaded RV which leads to its contractile failure. A large patch composed of collagen mixed with 10^7 cardiac Nkx2.5+ progenitors (CPC), gelatin and alginate polymerized with 100 mM Ca2+ was sunk in a mold with the size of the RV. The patch was surgically set on the epicardium through a right thoracotomy approach, to wrap the whole RV free wall of 8 pigs (CPC group). A control group (n=6) included pigs which received a cell-free patch. These patches are scalable and their stiffness (0.1 kPa) allowed an easy handling for the surgeons. The patch remains stuck to the epicardium without any suture after closure of the pericardium. Hydrocortisone (1mg/kg) was injected intravenously before closing to reduce inflammation. All animals were immunosuppressed by Tacrolimus (daily 0.3 mg/kg of Advagraft ®) from 10 days before cell therapy until euthanasia performed after a median delay of 86 ± 25 from cell therapy. Functional analysis was performed using RV echocardiographic standard and strain parameters in all animals at each step of protocol: at baseline before rTOF surgery, at 5 months before cell therapy and at 7 months at the end of study.

Echocardiography

Echocardiography was performed on closed-chest animals under general anesthesia in dorsal decubitus. We used commercially available Philips Epiq 7 ultrasound system with X5-1 matrix array transducer (Philips Healthcare) or a VIVID E9 (General Electric Medical System, Milwaukee, USA) equipped with a 2.5 Mhz (1.5-4.5) transducer. The values of all echocardiographic parameters were obtained as the average value of three consecutive cardiac cycles during transient apnoea. Measures were indexed to biological length (BL) or body surface area (BSA), calculated using the formula[5]

$$BSA_{(m^2)} = (Weight_{(kg)} \times Body\ Length_{(cm)})^{0.5} / 60$$

BL= √BSA

Echocardiographic measurements were determined as previously described[6].

In the parasternal long axis view, the RV anterior wall thickness and the ratio of RV/LV diastolic diameters were measured using TM mode. In the apical four-chamber view, RV end-diastolic and RV end-systolic areas were measured. This allowed the calculation of RV fractional area change (FAC), defined as followed:

FAC (%) = ([RV end-diastolic area – RV end-systolic area]/RV end-diastolic area)*100.

Tricuspid Annular Plane Systolic Excursion (TAPSE) was measured as the maximal excursion of the lateral annulus in the apical four-chamber view using M-mode recording through the apex of the RV and the junction between the RV free wall and the tricuspid annulus. Peak systolic velocity of S'wave (Peak S') was measured at the lateral tricuspid annulus using pulsed tissue Doppler imaging. From a parasternal short axis view, pulmonary annulus diameter and transpulmonary gradient through the pulmonary band were both measured by continuous-wave Doppler flow at the maximal pulmonary valve opening during systole. The presence of a diastolic flow reversal of color Doppler flow in the main or the branch pulmonary arteries was used to predict severe pulmonary regurgitation.

Among the echocardiographic measures, RV end-diastolic and end-systolic area, PA-diameter, RV/LV ratio and the tricuspid/mitral (TM) valve diameter ratio reflected RV dilation whereas the mean trans-pulmonary gradients were used to reflect the RV pressure overload. Finally, FAC, TAPSE and Peak S' represented overall RV systolic function.

Regarding the speckle tracking analysis, RV longitudinal deformation was measured by standard 2D grey-scale acquisitions. The peak longitudinal strain (LS) values were computed automatically, generating regional data from six segments of RV and an average value for apical 4-chamber. The peak LS was also assessed by a semi-automatic contouring of the endocardium of the free wall (FW), excluding the interventricular septum to minimize the

influence of the interventricular dependence. The peak global RV FW strain was defined as the average of the three FW segments. Peak LS is a negative value, but for ease of interpretation in comparing serial LS values, we have expressed LS as an absolute value. All images were recorded at a frame rate of 50-80 frames per second were stored for postprocessing analysis with QLAB 10 CMQ (Philips) advanced quantification software (EchoPAQ, 110.1.2 GE Healthcare, Horten, Norway)

Clinical status was evaluated daily during the study. Histologic analyses were performed on each animal at the end of the procedure.

Histology, Immunofluorescence Antibodies

Histology and Indirect immunofluorescence were performed on free wall and HD-area frozen sections. Fibrosis was stained by Sirius red (Sigma-Aldrich, France).

Immunofluorescence used anti–human nuclear KU80 antigen (Cell signaling Technology, C48E7) or anti human mitochondria antibody (anti-CoxIV, abcam ab197491) to detect human progenitor cells, anti-NKX2.5 (R&D AF2444), anti-sarcomeric actinin (Sigma-Aldrich clone E453), anti-NFκB (Cell Signaling Technology, 8242), anti OCT4 (Santa-Cruz Biotechnology rabbit anti-Oct4). Anti-Iba1 antibody (GTX89792) was from GeneTex.

Genomic DNA was prepared from RV free wall and HD-area pieces using the Wizard® Genomic DNA Purification Kit (Promega, France). Samples were submitted to polymerase chain reaction analysis, to quantify the presence of human cells using amplification of human ALU sequences. The negative control DNA was isolated from sham RV pieces.

Real time PCR

RNA was extracted from samples with a Quick RNA miniprep kit (Zymo Research, Ozyme, France). QPCR was performed using the LightCycler® FastStart DNA Master PLUS SYBR Green I kit and a light cycler 2.0 (Roche Life Science, France) as previously reported [7]

The primers used were:

HuMMP-1-F	*CCTAGCTACACCTTCAGTGG*
HuMMP-1-R	*GCCCAGTACTTATTCCCTTT*
HuMMP-3-F	*AGCAAGGACCTCGTTTTCATT*
HuMMP-3-R	*GTCAATCCCTGGAAAGTCTTCA*
HuMMP-9-F	*TACCCTATGTACCGCTTCAC*
HuMMP-9-R	*GAACAAATACAGCTGGTTCC*
huTIMP-1F	*AGTCAACCAGACCACCTTATACCA*
huTIMP-1R	*TTTCATAGCCTTGGAGGAGCTGGTC*
huTIMP-3F	*ACGATGGCAAGATGTACACAGG*
huTIMP-3R	*GGAAGTAACAAAGCAAGGCAGG*
Sus Col1a2- F	*GCACGTCTGGTTAGCAGA*
Sus Col1a2-R	*TGGTAGGTGATGTTTTGGGAC*
Sus Col3a1-F	*AGAGCGGAGAATATTGGGTTG*
Sus Col3a1-R	*CTTACGTGGAGTAGAAGGAC*
Sus Postn-F	*GACGAGGGAAGAACGAATCA*
Sus Postn-R	*TAAATGACCATCGCCACC*
Sus Acta2-F	*CAGGCAGGATGTGTGAAGAA*
Sus Acta2-R	*TCACCCCCTGATGTCTAGGA*
Sus TGFb1-F	*TTTCTGGTGGGGAGACAGAC*
Sus TGFb1-R	*CTCCCCTAGGCTGCTTTCTT*

Regulations

All experiments were carried out according to the European Community guiding principles in the care and use of animals (2010/63/UE, 22 September 2010), the local Ethics Committee guidelines and the French decree n°2013-118 on the protection of animals used for scientific purposes (JORF n°0032, 7 February 2013 p2199, text n°24). Authorization to perform animal experiments according to this decree was obtained from the Ministère Français de l'Agriculture, de l'Agroalimentaire et de la Forêt (agreement N° B92-019-01).

REFERENCES

1 Grey, C., Mery, A. & Puceat, M. Fine-tuning in Ca2+ homeostasis underlies progression of cardiomyopathy in myocytes derived from genetically modified embryonic stem cells. *Human molecular genetics* **14**, 1367-1377, doi:10.1093/hmg/ddi146 (2005).

2 Jebeniani, I., Ding, S. & Puceat, M. Improved Protocol for Cardiac Differentiation and Maturation of Pluripotent Stem Cells. *Methods Mol Biol* **1994**, 71-77, doi:10.1007/978-1-4939-9477-9_6 (2019).

3 Puceat, M., Roche, S. & Vassort, G. Src family tyrosine kinase regulates intracellular pH in cardiomyocytes. *The Journal of cell biology* **141**, 1637-1646, doi:10.1083/jcb.141.7.1637 (1998).

4 Lambert, V. *et al.* Right ventricular failure secondary to chronic overload in congenital heart disease: an experimental model for therapeutic innovation. *The Journal of thoracic and cardiovascular surgery* **139**, 1197-1204, 1204 e1191, doi:10.1016/j.jtcvs.2009.11.028 (2010).

5 Wang, J. & Hihara, E. A unified formula for calculating body surface area of humans and animals. *Eur J Appl Physiol* **92**, 13-17, doi:10.1007/s00421-004-1074-9 (2004).

6 Hodzic, A. *et al.* Standard and Strain Measurements by Echocardiography Detect Early Overloaded Right Ventricular Dysfunction: Validation against Hemodynamic and Myocyte Contractility Changes in a Large Animal Model. *J Am Soc Echocardiogr* **30**, 1138-1147 e1134, doi:10.1016/j.echo.2017.07.003 (2017).

7 Blin, G., Neri, T., Stefanovic, S. & Puceat, M. Human embryonic and induced pluripotent stem cells in basic and clinical research in cardiology. *Current stem cell research & therapy* **5**, 215-226, doi:10.2174/157488810791824584 (2010).